Positron Emission Tomographic imaging of tumor cell death using Zirconium-89-labeled APOMAB® Following Cisplatin Chemotherapy in Lung and Ovarian Cancer Xenograft Models

Vasilios Liapis (Vasilios.Liapis@sa.gov.au)
Centre for Cancer Biology https://orcid.org/0000-0002-2354-3521

William Tieu
South Australian Health and Medical Research Institute (SAHMRI) and the University of Adelaide

Nicole Wittwer
Centre for Cancer Biology, SA Pathology and University of South Australia

Tessa Gargett
Centre for Cancer Biology, SA Pathology and University of South Australia

Andreas Evdokiou
Basil Hetzel Institute and Centre for Personalised Cancer Medicine, University of Adelaide

Prab Takhar
South Australian Health and Medical Research Institute

Stacey E. Rudd
School of Chemistry and Bio21 Molecular Science and Biotechnology Institute

Paul S. Donnelly
School of Chemistry and Bio21 Molecular Science and Biotechnology Institute

Michael P. Brown
Centre for Cancer Biology, SA Pathology and University of South Australia, University of Adelaide, Royal Adelaide Hospital

Alexander H. Staudacher
Centre for Cancer Biology, SA Pathology and University of South Australia, University of Adelaide

Original research

Keywords: Zirconium-89, chimeric DAB4, Chemotherapy, Ovarian Cancer, Lung Cancer

Posted Date: June 3rd, 2020

DOI: https://doi.org/10.21203/rs.3.rs-32059/v1

Version of Record: A version of this preprint was published at Molecular Imaging and Biology on July 6th, 2021. See the published version at https://doi.org/10.1007/s11307-021-01620-1.

Abstract

Purpose. There are no currently approved non-invasive methods for detecting tumor treatment responses within the first few days of treatment. The monoclonal antibody, DAB4, or its chimeric derivative, chDAB4 (APOMAB®), targets the Lupus-associated or Sjögren Syndrome-B antigen (La/SSB). La/SSB is over-expressed in malignancy and is selectively targeted by chDAB4 in cancer cells dying after DNA-damaging treatment. Therefore, chDAB4 is a unique diagnostic tool that specifically detects dead cancer cells and could be used to distinguish between chemotherapy responsive and non-responsive patients. In this study, we performed preclinical validation studies using whole-body Positron-Emission Tomography (PET) to examine tumor and normal tissue uptake of ^{89}Zr-labeled chDAB4 in lung or ovarian tumor-bearing mice, which were left untreated or given cisplatin chemotherapy.

Methods. The binding of chDAB4 and its conjugates to dead cisplatin-treated human lung and ovarian cancer cells was assessed *in vitro* as well as its Fc-dependent effector functions. Mice bearing xenografts of H460 lung cancer or A2780 ovarian cancer cells were untreated or given cisplatin chemotherapy followed 24 hours later by ^{89}Zr-labeled chDAB4. Post-cisplatin tumor responses were monitored using bioluminescence imaging and caliper measurements and ^{89}Zr-labeled chDAB4 tumor uptake was measured using an Albira SI PET imager and PMOD analysis software. On completion of experiments, organs were dissected and biodistribution of ^{89}Zr-labeled chDAB4 was measured using a Hidex gamma-counter.

Results. The chDAB4 antibody bound only to dead A2780 and H460 cells, and its binding increased with cisplatin treatment *in vitro*. The chDAB4 antibody did not exhibit Fc-dependent effector functions. Chemotherapy significantly increased uptake of ^{89}Zr-labeled chDAB4 in tumors but not in normal tissues for each tumor model. The greatest differences in average uptake of ^{89}Zr-labeled chDAB4 in subcutaneous tumors were observed 3 days post-cisplatin chemotherapy compared to untreated mice, and before tumor shrinkage was evident.

Conclusion. After administration of cisplatin chemotherapy, tumor xenograft uptake of ^{89}Zr-labeled chDAB4 was detected *in vivo* by PET imaging. Given that the chDAB4 mAb lacked effector activity and that malignant rather than normal tissues were targeted after chemotherapy, these results support clinical development of chDAB4 as both a predictive marker of chemotherapy response and a theranostic imaging agent, which may guide subsequent delivery of chDAB4-directed antibody drug or radio-conjugate anticancer therapies.

Introduction

The care and treatment of cancer patients places an intense demand on healthcare systems globally. Standard treatment regimens for locally advanced or metastatic cancers usually employ radiotherapy, cytotoxic chemotherapy or both. Often, however, the treatment is not sufficiently effective and may represent a significant personal and socioeconomic burden for patients if it is both toxic and ineffective.

Therefore, a robust method for early or interim determination of tumor responses may allow patients to continue effective therapy, discontinue ineffective therapy and also aid in go/no-go decision making in anticancer drug development.

Current methods for determining tumor responses are based on measuring changes in tumor dimensions using computed tomography (CT), magnetic resonance imaging (MRI) and ultrasound according to Response Evaluation Criteria in Solid Tumors (RECIST) [1] or measuring FDG avidity on ^{18}F-FDG positron emission tomography (PET)/(PET/CT) scans using PET Response Criteria in Solid Tumors (PERCIST) or tumor-specific criteria [2, 3]. Although there is no established role for FDG-PET in chemotherapy response monitoring of either lung or ovarian cancers [4, 5], FDG-PET and SPECT studies in non-small cell lung carcinoma (NSCLC) patients after a first cycle of platinum-based chemotherapy have been informative. For example, tumor responders, who were defined as having a decrease of at least 10% in standardized uptake value (SUV) of tumor FDG uptake, had the best survival prospects [5, 6]. In NSCLC patients who received ^{99m}Tc-labeled annexin V as a marker of cell death, early chemotherapy-induced tumor-specific annexin V uptake on SPECT significantly correlated with later RECIST-defined tumor responses although some patients with RECIST-defined stable disease also had tumor annexin V uptake [7]. Nevertheless, the sensitivity and specificity of FDG-PET/CT for therapy response monitoring may be limited by such tumor variables as expression of glucose transport exporters [8] or tissue inflammation or infection both of which may also be FDG avid [9]. Therefore, there has been great interest in the field of molecular imaging to develop selective, robust, and clinically applicable *in vivo* imaging markers of therapy-induced tumor cell death [10–12].

Among the cited *in vivo* imaging markers of therapy-induced tumor cell death that may have these qualities is DAB4 (APOMAB®), which is a mouse monoclonal antibody (mAb) and which has been reformulated as a chimeric mAb (chDAB4). The mAb, DAB4/chDAB4, targets the ubiquitously and abundantly expressed ribonucleoprotein, Lupus-associated (La)/Sjögren Syndrome-B (SSB) antigen which is overexpressed in many different cancers [13–15]. La/SSB only becomes accessible for antibody binding in cells that have lost membrane integrity, particularly in apoptotic and necrotic cancer cells, making DAB4 a dead tumor cell–targeting mAb, particularly after DNA-damaging anticancer treatment [16, 17]. The La/SSB protein is highly conserved between mice and humans and DAB4 binds to both mouse and human forms of La/SSB. As well as *in vitro* studies, we have shown that DAB4 binds with high specificity to dead tumor cells *in vivo.* We drew on this tumor-targeting property to radiolabel DAB4 with ^{111}Indium for tumor imaging [18, 19] and with ^{90}Yttrium [17], ^{177}Lutetium [20] and ^{227}Thorium [21] for antitumor therapy by exploiting the phenomenon of β- and α-radiation crossfire [22].

In preparation for an imminent clinical theranostic imaging trial, the murine DAB4 $F(ab)_2$ region has been genetically fused to the human IgG1 Fc to generate chimeric DAB4 (chDAB4). We radiolabeled chDAB4 with the positron-emitting radionuclide Zirconium-89 ($[^{89}Zr]Zr^{IV}$) so that the radioimmunoconjugate could be used for non-invasive PET imaging. Zirconium-89 is a residualizing radionuclide that has been used extensively for radiolabeling antibodies for clinical immuno-PET studies [23, 24]. The physical half-life of

Zirconium-89 of 3.3 days is similar to the biological half-life of mAbs, so the radionuclide is well suited for radiolabeling mAbs, making it possible to obtain PET images with desirable contrast between tumor uptake and normal tissue background.

In this study, the ability of [^{89}Zr]Zr-chDAB4 to selectively bind to dead tumor cells in human xenografts of lung and ovarian cancer after chemotherapy was examined using PET imaging. This preclinical validation study supports the use of chDAB4 as a diagnostic tool for detecting tumor responses to first line platinum-based chemotherapy in lung and ovarian cancer patients.

Materials And Methods

Cell culture and antibodies

The A2780 ovarian cancer cell line was purchased from ATCC (USA) and the H460 large cell lung carcinoma cell line was a gift from Associate Professor Carleen Cullinane (Peter MacCallum Cancer Centre, Australia). Both lines were authenticated by short tandem repeat testing using the AmpFISTR Identifier Kit (ThermoFisher Scientific) by SA Pathology (Adelaide, South Australia). All cell lines were cultured in RPMI-1640 which contained penicillin and streptomycin (Sigma-Aldrich), 10% foetal calf serum (FCS) (Bovogen Biologicals, Victoria, Australia). Cells were negative for mycoplasma contamination using MycoAlert® Mycoplasma Detection Kit (Lonza, Basel, Switzerland). The generation of luciferase tagged H460 and A2780 cells was performed as described previously [25–27]. Chimeric DAB4 (chDAB4), resulting from the genetic fusion of the murine DAB4 F(ab)$_2$ and human IgG1 (huIgG1) Fc, was produced as previously described [28]. The CH2 domain of chDAB4's huIgG1 Fc harbors the K322A mutation, which can abrogate complement-dependent cytotoxicity (CDC) and attenuate antibody-dependent cytotoxicity (ADCC) [29].

Flow cytometry analysis of chDAB4 binding to H460 and A2780 cells

A2780 and H460 cells were treated with increasing concentrations of cisplatin (Hospira, Australia) for 48 hours, collected, washed with FACS buffer (2.5% BSA, 0.04% sodium azide in PBS) and incubated with 5 µg/mL chDAB4 or human IgG (Intragram P; as control) for 30 minutes. Cells were washed and incubated with 2 µg/mL goat anti-human IgG Alexa Fluor® 647 (ThermoFisher Scientific, USA) for 20 minutes, washed further, incubated with 0.5 µg/mL Propidium Iodide (PI) (Sigma-Aldrich) and analyzed by flow cytometry using a BD Accuri flow cytometer (BD Biosciences, Franklin Lakes, NJ, USA). Gating was set at 2% positive events in the isotype control sample. Specific binding was calculated as the difference in Mean Fluorescence Intensity (MFI) between chDAB4 and the isotype control antibody and expressed as the net MFI, which was calculated from triplicate samples.

Chelator conjugation and radiolabeling of chDAB4 with ^{89}Zr

[^{89}Zr]Zr^{IV} oxalate was produced by SAHMRI via proton irradiation of a ^{89}Y target on a PETtrace 880 cyclotron (GE Healthcare) and purified on an Alceo solid target processing system (Comecer, Italy) as described previously [30]. The chDAB4 mAb was conjugated to the bifunctional chelator *p*-isothiocyanatobenzyl-deferoxamine (DFO-*p*Phe-NCS) (Macrocyclics, Texas, USA) and radiolabeled with [^{89}Zr]Zr^{IV} as described previously [31]. The radiolabeled antibody was washed and concentrated using 100 kDa MWCO centrifuge filters and resuspended in sterile PBS for injection. Instant thin layer chromatography (ITLC) with 25 mM citrate buffer (pH 5.5) as a mobile phase was used to measure the amount of free [^{89}Zr]Zr^{IV} in the preparation, which was < 1% of total activity (R_f <0.2 [bound [^{89}Zr]Zr^{IV}] *vs* R_f >0.7 [free [^{89}Zr]Zr^{IV})]).

Cell binding assays

A modified version of the Lindmo binding assay [32] was used to determine the immunoreactive fraction (IRF) of the radiolabeled chDAB4. H460 human lung cancer cells were fixed and permeabilized as previously described [16, 17], resuspended in PBS with 1% FCS and serially diluted from 5×10^7 to 3.9×10^6 cells in 0.5 mL performed in duplicate. 500 ng/mL of radiolabeled antibody in 0.5 mL PBS with 1% FCS was added to the cell suspensions and incubated at 4˚C overnight. The cells were pelleted by centrifugation at 300 *g* and 0.5 mL of the supernatant from each sample was placed in a separate tube. The radioactivity in the cell pellets and the supernatant was measured using an Automatic Gamma Counter (Hidex, Finland). The inverse cell concentration (mL/cells in sample) was plotted against the total activity (activity in supernatant + activity in pellet)/specific binding (total bound) and the linear regression was extrapolated to calculate interception of the y-axis where x = 0 and expressed as a percentage (IRF = 100% × 1/y[x = 0]).

The binding affinity of conjugated and radiolabeled chDAB4 was compared to the intact, unlabeled chDAB4 using a La/SSB-specific ELISA as described previously [33].

In vitro assays for complement dependent cytotoxicity (CDC), antibody dependent cellular cytotoxicity (ADCC) and cytokine release

In the CDC assay, CD20$^+$ Raji cells purchased from CellBank (Australia) or CD20$^-$ Jurkat cells kindly provided by Professor Andrew Zannettino (Myeloma Research Laboratory, University of Adelaide, Australia) were harvested, washed and added to each well of a 96-well U-bottom plate at 10^5 cells/well in RPMI-1640 with 10% rabbit serum as the source of complement. The CD20-specific chimeric mAb, rituximab, was used as a positive control, and medium alone and the EGFR-specific chimeric mAb, cetuximab, were used as negative controls. The mAbs were added at a concentration of 15, 1.5, 0.15 or 0.015 µg/mL in RPMI-1640 with 10% rabbit serum and incubated for 2 hours at 37˚C. Thiazolyl Blue Tetrazolium Bromide at a final concentration of 0.4 mg/mL was added per well and the plate incubated for another 1 hour at 37˚C with 5% CO_2. The plate was centrifuged at 300 *g* for 3 minutes, the supernatant was removed, and the resulting crystals resuspended in 150 µL isopropanol. Absorbance was measured at 570 nm using a FLUOStar Omega plate reader.

ADCC was examined using the Promega ADCC Reporter Bioassay kit. The assay uses genetically modified Jurkat effector cells, which stably express the high-affinity V158F receptor variant of FcγRIIIa together with a reporter gene construct comprising a nuclear factor of activated T-cells (NFAT) response element driving firefly luciferase expression. Binding to FcγRIIIa via the mAb Fc domain may result in detectable luciferase expression and induction of ADCC. $CD20^+$ Raji cells were used as the target cells. Permeabilized H460 cells, which are strongly bound by chDAB4, were also used as target cells. In a 96-well plate, chDAB4 or rituximab were added at 3 µg/mL in triplicate. The antibodies were serially diluted 1:2.5 to achieve final concentrations of 0, 0.002, 0.005, 0.012, 0.03, 0.08, 0.19, 0.48, 1.2, or 3 µg/mL. The target cells were added to each well followed by effector cells and incubated for 6 hours with 5% CO_2 at 37˚C. Plates were equilibrated to room temperature for 15 minutes before the Bio-Glo Luciferase Assay Reagent was added, incubated for 45 minutes and luminescence measured using a FLUOstar Omega plate reader.

For the cytokine release assay (CRA), fresh blood was taken from five normal volunteer donors. Peripheral blood mononuclear cells (PBMCs) were isolated using density gradient centrifugation with Lymphoprep (Alere Technologies) as per manufacturer's instructions and seeded at 10^5 cells/well in a 96-well U-bottom plate. In duplicate, cells were treated with increasing doses of chDAB4 or 15 µg/mL anti-CD3 antibody (clone OKT3; prepared in-house) as a positive control for 24 hours at 37˚C with 5% CO_2. The following day, cells were pelleted and 100 µL of supernatant per well was analyzed for cytokine levels using the LEGENDplex Human Inflammation Panel 1 (Biolegend) following the manufacturer's instructions.

Animal experiments

For the A2780 and H460 tumor models, 6-10-week-old female NOD *scid* gamma-null (NSG) mice were inoculated subcutaneously in the right flank with 5×10^6 tumor cells in a 1:1 ratio of Matrigel/PBS. For the intraperitoneal ovarian cancer model, 5×10^6 cells in 100 µL PBS were injected into the intraperitoneal cavity.

The IVIS® Spectrum Imaging system (PerkinElmer, Massachusetts, USA) was used for non-invasive monitoring of tumor growth of the luciferase-expressing cell lines. Mice were given intraperitoneal injections (i.p.i.) with 100 µL of D-Luciferin solution at 150 mg/kg (Pierce Biotechnology, IL, USA) and then gas-anesthetized with isoflurane (Veterinary Companies of Australia, NSW, Australia). Images were acquired for 1–30 seconds (representative images are shown at 1 second, 20 minutes after D-Luciferin by i.p.i.) and the photon emission transmitted from mice was captured and quantified as photons/sec/cm^2 using Living Image Software (version 4.7.2; Perkin Elmer, Massachusetts, USA). Tumor growth was also measured using electronic calipers with tumor volume determined using the calculation $(a^2 \times b)/2$, where a is the shortest diameter and b is the longest diameter of the tumor.

Mice were randomly allocated to treatment groups when the subcutaneous tumors reached approximately 50 mm^3, or 7 days after intraperitoneal injection of A2780 cells. Mice were untreated or

treated by i.p.i. with 4 mg/kg cisplatin on Day 0. After chemotherapy on Day 1, mice bearing subcutaneous tumors were given 6 MBq/50 µg [^{89}Zr]Zr-chDAB4 by intravenous injection (i.v.i.) while mice bearing ascitic A2780 tumors were given 6 MBq/75 µg of [^{89}Zr]Zr-chDAB4 by i.v.i. As a blocking control, mice bearing H460 tumors were given 250 µg of unlabeled chDAB4 1 hour by i.v.i. before the ^{89}Zr-chDAB4 injection. Mice were monitored daily and tumor volume measured at least three times per week via bioluminescence imaging and caliper measurement. At the end of the experiment, mice were humanely killed, and organs were removed, weighed and counts were measured with the background and decay corrected using a Hidex gamma-counter for accumulation of ^{89}Zr.

In vivo PET and MRI scanning

Mice were anesthetized with 2% isoflurane and scanned for 10 minutes using the Albira Si PET-SPECT small animal scanner (Bruker Biospin GmbH, Valencia, Spain), with a submillimetric resolution of 0.7 mm. Regions of interest were manually selected from the maximum intensity projections (MIPs) and were used to analyze the radiotracer accumulation within the tumor using the PMOD imaging suite (PMOD technologies, Switzerland). At the end of the study, 2 mice with intraperitoneal A2780 tumors underwent MRI imaging using the T2 weighted RARE spin echo sequence on the Bruker Icon 1T benchtop MRI system. The ITK Snap software was used to segment the scans [34].

Statistical analysis

Statistical analyses were performed using GraphPad Prism (v7.0) software. Comparison of groups was performed by two-way *t*-test or intergroup comparisons made by two-way Analysis of Variance (ANOVA). Data are shown as mean ± Standard Error of the Mean (SEM) or Standard Deviation (SD). Statistical significance was reached when $p < 0.05$, with * representing $p < 0.05$, ** $p < 0.01$, *** $p < 0.001$ and **** $p < 0.0001$.

Results

chDAB4 binds to cisplatin-treated dead H460 lung cancer cells and A2780 ovarian cancer cells **in vitro**

The A2780 and H460 cell lines were untreated or treated *in vitro* for 48 hours with increasing doses of cisplatin and the binding of chDAB4, or the human IgG control, to dead (PI^+) cells was assessed. For both cell lines, cisplatin treatment increased cell death in a dose-dependent manner (Fig. 1A). Cisplatin also increased the percentages of chDAB4-bound dead tumor cells and, at the highest dose of 10 µg/mL cisplatin, > 85% of H460 cells and 80% of A2780 cells were PI^+ and bound by chDAB4 (Fig. 1B). This dose-dependent increase in proportions of chDAB4-bound dead tumor cells was matched by proportionate increases in the per cell binding of chDAB4, which was measured as increasing mean fluorescence intensity (MFI) of dead tumor cell-bound chDAB4 with increasing cisplatin dose (Fig. 1C).

Validation of conjugation and radiolabeling of immunoreactive chDAB4

After DFO conjugation to the chDAB4 mAb as described by Vosjan *et al*. [31], analysis of the conjugate by electrospray ionization mass spectrometry revealed the conjugate had between 0–3 chelators attached per mAb with an average of 0.8 H_3DFO per antibody (Supplementary Fig. 1A). Radiolabeling of chDAB4 with [^{89}Zr]Zr^{IV}, resulted in specific activities ranging from 115 to 170 MBq/mg and < 1% free [^{89}Zr]Zr^{IV} in the preparation by ITLC (data not shown). The immunoreactive fraction was 88.3% as determined by the Lindmo assay (Supplementary Fig. 1B) and the binding to the La/SSB peptide epitope by each of unconjugated, conjugated or radiolabeled versions of chDAB4 measured by ELISA were similar (Supplementary Fig. 1B). The dissociation constant (Kd) values for unconjugated chDAB4, DFO-conjugated chDAB4 and the radioimmunoconjugate [^{89}Zr]Zr-DFO-chDAB4 measured as pmol/L (± SEM) were 17.8 ± 2.8, 19.7 ± 2.6 and 23.1 ± 3.9 respectively (Supplementary Fig. 1B). These data show that binding affinities were minimally altered by the processes of conjugation or radiolabeling.

Characterization of the immune effector properties of chDAB4

We investigated the immunologic properties of unconjugated chDAB4 using *in vitro* assays for CDC, ADCC and cytokine release. Although rituximab initiated the complement-mediated lysis of CD20$^+$ Raji target cells (but not CD20$^-$ Jurkat cells), neither of the other chimeric mAbs, chDAB4 and cetuximab, both of which contain huIgG1 Fc, resulted in cytotoxicity of the Raji cells (Supplementary Fig. 1C). Next, we used a reporter assay to measure the intracellular signaling that would be induced in cells mediating ADCC after exposure to antibody-bound target cells. In contrast to the induction of the reporter signal after exposure to rituximab-bound Raji cells, there was no signal induction either using as targets, the viable Raji or H460 cells that show minimal or no binding by chDAB4, or the permeabilized H460 cells that show high binding by chDAB4 (Supplementary Fig. 1C). Results of the *in vitro* cytokine release assay (Supplementary Fig. 1D) show a relative lack of reactivity of chDAB4 among PBMCs of 5 normal subjects and, in particular, no chDAB4-dose-dependent elevations in inflammatory cytokine levels were observed. One subject (#1), who was found to have had a concurrent systemic viral infection, had elevated baseline levels of some cytokines. Another subject (#2) had elevations of IL-6 and TNF-α that were independent of chDAB4 concentration.

[^{89} Zr]Zr-chDAB4 biodistribution and tumor uptake in untreated and cisplatin treated mice bearing subcutaneous xenografts of the human H460 lung cancer cell line

In the subcutaneous xenograft model of H460 lung cancer, cisplatin treatment significantly reduced tumor size as measured by bioluminescence imaging (Fig. 2A), calipers, and tumor weights at end of study (Fig. 2B). In cisplatin-treated mice compared to untreated mice, PET imaging starting the day after the [^{89}Zr]Zr-chDAB4 injection, which corresponds to 2 days post-cisplatin, showed increasing tumor uptake and reducing tissue background during the week post-injection (Fig. 2C), and before tumor growth delay became apparent (Fig. 2B). Analysis of [^{89}Zr]Zr-chDAB4 biodistribution either by PMOD PET imaging software or organ assay at the completion of the study showed significantly increased tumor uptake (Fig. 2D). To demonstrate tumor-specific targeting of [^{89}Zr]Zr-chDAB4, cisplatin-treated mice

received a five-fold excess (250 μg) of unlabeled chDAB4 one hour before the [^{89}Zr]Zr-chDAB4 injection. This prior 'cold' antibody treatment appreciably blocked tumor accumulation of [^{89}Zr]Zr-chDAB4 and prolonged blood-pool radioactivity (Fig. 2C). The physical biodistribution data (Fig. 2D) showed significantly greater mean tumor uptake (± SD) of [^{89}Zr]Zr-chDAB4 in cisplatin-treated mice of 26.7 ± 16.9%ID/g compared either to 13.1 ± 5.8%ID/g for untreated mice and 7.7 ± 4.0%ID/g for treated mice previously administered cold chDAB4 mAb.

Prior administration of unlabeled chDAB4 mAb to cisplatin-treated mice not only led to a significant reduction in tumor uptake of [^{89}Zr]Zr-chDAB4 in treated mice but also led to an increase in mean blood accumulation of [^{89}Zr]Zr-chDAB4 at the completion of the study, measured as %ID/g (± SD) (9.4 ± 1.6, blocking control; 4.3 ± 4.3, treated; and 2.1 ± 2.9, untreated) and a reduction in mean bone uptake (11.5 ± 1.2, blocking control; 20.7 ± 5.1, treated; and 19.5 ± 4.8, untreated). Interestingly, cisplatin-treated mice that were pre-administered blocking antibody also had a significant reduction in mean splenic uptake of radiolabeled antibody measured as %ID/g (63.2 ± 16.5, blocking control; 83.7 ± 30.5, treated; and 109.3 ± 28.9, untreated). Using PMOD software, data obtained over the 6-day PET imaging period confirm significantly greater tumor uptake of [^{89}Zr]Zr-chDAB4 in cisplatin-treated mice than either treated mice given prior blocking antibody or untreated mice with Day 3 having the greatest difference between the groups (%ID/g ± SD) 26.9 ± 4.9, 13.0 ± 1.6 and 17.6 ± 3.6 respectively (Fig. 2C).

[^{89} Zr]Zr-chDAB4 biodistribution in untreated and cisplatin-treated mice bearing subcutaneous and ascitic xenografts of the human A2780 ovarian cancer cell line.

In the subcutaneous A2780 ovarian cancer xenograft model, bioluminescence imaging illustrated that cisplatin treatment significantly controlled tumor growth compared to untreated control mice (Fig. 3A). The significant antitumor activity of cisplatin was also evident both as reduced tumor growth by caliper measurements and lower *ex vivo* tumor weights at the end of study (Fig. 3B), with the mean tumor weight (± SD) of cisplatin-treated mice being 196 ± 121.6 mg compared to 563 ± 164.3 mg in untreated mice.

Mice were imaged daily after injection of [^{89}Zr]Zr-chDAB4 from Day 1, the day after chemotherapy administration, and representative PET scans together with the extent of tumor uptake determined by PMOD PET image analysis are shown in Fig. 3C. These data show that tumor uptake of [^{89}Zr]Zr-chDAB4 significantly increased in treated mice at 2 and 3 days post-[^{89}Zr]Zr-chDAB4 injection, which corresponds to 3 and 4 days after chemotherapy was given on Day 0. Tumor uptake at 2 and 3 days post-[^{89}Zr]Zr-chDAB4 injection (± SD) was 49.3 ± 6.9 and 49.3 ± 8.3%ID/g, respectively, for cisplatin-treated mice compared to 37.9 ± 8.7 and 37.6 ± 8.8%ID/g, respectively, for untreated mice. Again, this tumor uptake of [^{89}Zr]Zr-chDAB4 in cisplatin-treated mice preceded the later observed delay in growth of the tumors (Fig. 3A). Organ assay at the completion of the study showed elevated tumor accumulation in treated mice, with no significant differences in uptake by normal tissues (Fig. 3D). As has been shown in other studies of immuno-incompetent NSG mice receiving radiolabeled antibodies [35–37], significant

accumulation of activity in the spleens of A2780 tumor-bearing mice was observed, regardless of prior chemotherapy.

As A2780 tumor cells can also be grown as ascitic tumors, A2780 cells were given by intraperitoneal injection to mice to reproduce the pattern of tumor growth commonly seen in ovarian cancer patients. Bioluminescence imaging was used to evaluate tumor growth because the ascitic tumors are not easily palpable. Representative whole-body bioluminescence images (Fig. 4A) and quantification of these data (Fig. 4B) showed a significant reduction in disease burden compared to untreated mice, particularly within the first few days after chemotherapy. At the completion of the experiment, mean tumor weight (± SD) in cisplatin-treated mice was smaller 168.8 mg (± 130) than in untreated mice 233.3 mg (± 348), but did not reach statistical significance (Fig. 4B). MRI imaging confirmed the presence of an intraperitoneal tumor for the mice shown in Fig. 4A and that the tumor was smaller after cisplatin treatment (Fig. 4C). Representative PET slices and the biodistribution of [^{89}Zr]Zr-chDAB4 measured as mean %ID/g (± SD) (Fig. 4D) indicated that tumor accumulation of [^{89}Zr]Zr-chDAB4 tended to be higher in cisplatin-treated mice, 30.3 ± 19.9%ID/g, than in untreated mice, 13.3 ± 4.4%ID/g, but did not reach statistical significance. The observed significant increase in intestinal accumulation of activity between untreated (36.3 ± 16.8%ID/g) and treated mice (12.5 ± 7.7%ID/g) is not consistent with chemotherapy-induced intestinal accumulation but rather may result from contamination of the intestinal samples by attached and untreated peritoneum-derived tumor material.

Discussion

This study provides preclinical proof of concept that detection of platinum-induced tumor cell death using the chDAB4 antibody corresponds to tumor growth delay and that radiolabeling chDAB4 with Zirconium-89 enables the non-invasive and longitudinal study of its biodistribution in live mice bearing lung and ovarian cancer xenografts. In current clinical oncology practice, interim responses to platinum-based chemotherapy may not be determined by CT scanning until after 2 or 3 cycles of chemotherapy (equivalent to 9 or 12 weeks), which may mean that patients experience chemotherapy side effects without realizing a clinical benefit [38]. Here, our whole-body PET imaging studies with [^{89}Zr]Zr-labeled chDAB4 using *in vivo* models of cisplatin-sensitive human ovarian and lung cancers [39, 40] show for the first time an early indication of tumor response after a single dose of cisplatin chemotherapy.

The results of the *in vitro* CDC, ADCC and cytokine release assays [41] demonstrate that the chimeric version of DAB4, which contains the K322A mutation in the CH2 domain of its huIgG1 Fc [29], lacks significant immune effector activity that might compromise its safety as a clinical theranostic imaging agent. This finding lends support to our use of chDAB4 in an IRB-approved phase 1 clinical immunoPET trial of [^{89}Zr]Zr-labeled chDAB4, which will commence soon in advanced lung and ovarian cancer patients who will receive their first cycle of platinum-based chemotherapy (Australian and New Zealand Clinical Trials Registry submission #379693).

The post-chemotherapy patterns of tumor uptake observed with [^{89}Zr]Zr-labeled chDAB4 in the biodistribution studies are consistent with results of previous biodistribution studies in murine tumor models using ^{14}C-, ^{111}In-, or ^{177}Lu-labeled versions of the parental murine DAB4 mAb [20]. In these studies, post-chemotherapy tumor accumulation of DAB4 was rapid, antigen-specific and associated with the extent of chemotherapy-induced tumor cell death. Notwithstanding the effect of the prior step of DNA-damaging chemotherapy on tumor uptake of DAB4, there was no evident accumulation of DAB4 in chemo-sensitive normal tissues such as intestine.

Our investigation of antibody drug conjugates of chDAB4 demonstrated that chDAB4-bound dead lung cancer cells could be phagocytosed *in vitro* by macrophages and suggested that similar macrophage-mediated processing of chDAB4 may occur *in vivo* [33]. The significantly reduced bone uptake of [^{89}Zr]Zr^{IV} after prior blockade with unlabeled chDAB4 indicates that less free bone-seeking [^{89}Zr]Zr [42] is generated within the body of each mouse and this result may thus help to explain the significantly higher blood activity level. These data suggest that catabolism of [^{89}Zr]Zr-labeled chDAB4 is required to release free or chelator-bound [^{89}Zr]Zr^{IV} and we hypothesize that tumor associated macrophages are likely to be one of the major catabolizing cell types.

Our biodistribution results also indicate that significant bone uptake of ^{89}Zr was observed in each of the three xenograft tumor models. We administered [^{89}Zr]Zr-labeled chDAB4 equivalent to a protein mass of between 50 µg and 75 µg and we observed bone uptake of [^{89}Zr]Zr^{IV} irrespective of the use of chemotherapy. Even administration of as little as 0.31 MBq/5 µg [^{89}Zr]Zr-labeled DS-8273a, which is a death receptor 5 targeting antibody, results in double the bone uptake of radionuclide compared to ^{111}In-labeled DS-8273a [43]. Moreover, bone uptake of [^{89}Zr]Zr after administration of [^{89}Zr]Zr-labeled mAbs can confound the interpretation of immunoPET images by potentially creating false positive osseous lesions [44].

The commercially available DFO-*p*Phe-NCS bifunctional chelator used in this study may have reduced *in vivo* stability [45, 46], thus contributing to bone accumulation of activity. However, new chelators are being developed and may improve the stability and biodistribution of ^{89}Zr-labeled mAbs such as [^{89}Zr]Zr-chDAB4, which can generate free [^{89}Zr]Zr^{IV} and result in its uptake by bone. For example, Donnelly *et al.* compared their novel chelator DFO-Sq to DFO-*p*Phe-NCS using the HER2-targeting antibody, trastuzumab [47] and Raave *et al.* also indicated greater stability and less bone accumulation when DFOcyclo was used in preference to DFO to radiolabel trastuzumab with [^{89}Zr]Zr^{IV} [48]. Consequently, the stability of the chelator together with the activity and antibody concentration [49] of [^{89}Zr]Zr-labeled mAbs will be important parameters to consider in planning future clinicals of [^{89}Zr]Zr-labeled chDAB4.

Finally, [^{89}Zr]Zr-labeled chDAB4 may be used in radiation dosimetry [50] in order to determine subsequent dosing regimens for chDAB4 to be employed in clinical antibody radioconjugate therapy based on our previous preclinical data [17]. Now that cytotoxic chemotherapy is a component of standard frontline chemo-immunotherapy regimens for advanced NSCLC patients [51, 52], tumor-targeted internal

radiotherapy such as that delivered by chDAB4 may lead to interactions with immune checkpoint inhibitor therapy and potentially promote the antitumor activity of the combination regimen [53].

Conclusion

Using mice bearing tumor xenografts of lung and ovarian cancer, we show specific and significantly increased and early tumor binding of the [^{89}Zr]Zr-radiolabeled chimeric DAB4 monoclonal antibody, which had been administered the day after a single dose cisplatin chemotherapy. In keeping with previously published *in vitro* and *in vivo* data, *in vitro* binding studies indicated that [^{89}Zr]Zr-chDAB4 bound dead tumor cells in a cisplatin dose-dependent manner. Longitudinal PET imaging showed that tumor localized [^{89}Zr]Zr-chDAB4 was detected before delayed tumor growth became evident. We validated that the chDAB4 mAb lacked significant immune effector activity. Together, these results yield preclinical proof-of-concept for [^{89}Zr]Zr-chDAB4 immunoPET and suggest that this method provides useful theranostic information to enable early and reliable detection of interim tumor responses to the platinum-based chemotherapy that is the mainstay of firstline systemic treatment regimens for patients with advanced lung or ovarian cancers. We plan to test this concept clinically using [^{89}Zr]Zr-chDAB4 immunoPET.

Abbreviations

ADCC
antibody-dependent cytotoxicity; ANOVA:Analysis of Variance; CDC:complement-dependent cytotoxicity; CRA:Cytokine Release Assay; CT:computed tomography; IRF:immunoreactive fraction; %ID/g:% Injected Dose per Gram; i.p.i:intraperitoneal injections; ITLC:Instant thin layer chromatography i.v.i:intravenous injection; La/SSB:Lupus-associated or Sjögren Syndrome-B antigen; MFI:Mean Fluorescence Intensity; MIP:maximum intensity projection; MRI:magnetic resonance imaging; NFAT; nuclear factor of activated T-cells; NSCLC:non-small cell lung carcinoma; NSG:NOD *scid* gamma-null; PET:Positron-Emission Tomography; PERCIST:PET Response Criteria in Solid Tumors; PI:Propidium Iodide; RECIST:Response Evaluation Criteria in Solid Tumors; SD:Standard Deviation SEM:Standard Error of the Mean; SUV:standardized uptake value; [^{89}Zr]Zr^{IV}:Zirconium-89.

Declarations

Ethics approval: The SAHMRI Animal Ethics Committee, (Adelaide, Australia) approved all animal experiments, which were conducted following institutional ethical guidelines.

Consent for Publication: Not Applicable

Availability of data and materials: The datasets generated during and/or analysed during the current study are available from the corresponding author on reasonable request.

Competing interest: MPB is co-inventor on APOMAB® patents owned by AusHealth Research Pty Ltd. No other competing interests relevant to this article exist.

Funding: This study was funded by AusHealth Research Pty Ltd, Adelaide, National Health and Medical Research Council, Australia (Project Grant ID 1126304)

Authors' contributions: VL, MPB and AHS contributed to the study conception and design. Material preparation, data collection and analysis were performed by VL, WT, NW, TG, AE, SER, PSD and AHS. The first draft of the manuscript was written by VL and MPB and AHS contributed to major revisions of the manuscript. All authors read and approved the final manuscript.

Acknowledgments The authors acknowledge the facilities and technical assistance provided via Dr Marianne Keller of the National Imaging Facility, a National Collaborative Research Infrastructure Strategy (NCRIS) initiative and the staff in the Bioresources department of the South Australian Health and Medical Research Institute (SAHMRI). We acknowledge Mass Spectrometry and Proteomics Facility (MSPF) at Bio21 institute, University of Melbourne for the use of mass spectrometer and HPLC systems.

References

1. Eisenhauer EA, Therasse P, Bogaerts J, Schwartz LH, Sargent D, Ford R, et al. New response evaluation criteria in solid tumours: Revised RECIST guideline (version 1.1). Eur J Cancer. 2009;45:228–47. doi:10.1016/j.ejca.2008.10.026.
2. Wahl RL, Jacene H, Kasamon Y, Lodge MA. From RECIST to PERCIST: Evolving Considerations for PET Response Criteria in Solid Tumors. J Nucl Med. 2009;50:122S-50S. doi:10.2967/jnumed.108.057307.
3. Peacock JG, Christensen CT, Banks KP. RESISTing the Need to Quantify: Putting Qualitative FDG-PET/CT Tumor Response Assessment Criteria into Daily Practice. American Journal of Neuroradiology. 2019;40:1978–86. doi:10.3174/ajnr.A6294.
4. Gallamini A, Zwarthoed C, Borra A. Positron Emission Tomography (PET) in Oncology. Cancers. 2014;6:1821–89. doi:10.3390/cancers6041821.
5. Gerke O, Ehlers K, Motschall E, Hoilund-Carlsen PF, Vach W. PET/CT-Based Response Evaluation in Cancer-a Systematic Review of Design Issues. Molecular imaging biology. 2020;22:33–46. doi:10.1007/s11307-019-01351-4.
6. Weber WA, Petersen V, Schmidt B, Tyndale-Hines L, Link T, Peschel C, et al. Positron emission tomography in non-small-cell lung cancer: prediction of response to chemotherapy by quantitative assessment of glucose use. J Clin Oncol. 2003;21:2651–7. doi:10.1200/jco.2003.12.004.
7. Kartachova M, van Zandwijk N, Burgers S, van Tinteren H, Verheij M, Valdes Olmos RA. Prognostic significance of 99mTc Hynic-rh-annexin V scintigraphy during platinum-based chemotherapy in advanced lung cancer. J Clin Oncol. 2007;25:2534–9. doi:10.1200/jco.2006.10.1337.

8. Alakus H, Batur M, Schmidt M, Drebber U, Baldus SE, Vallbohmer D, et al. Variable 18F-fluorodeoxyglucose uptake in gastric cancer is associated with different levels of GLUT-1 expression. Nucl Med Commun. 2010;31:532–8. doi:10.1097/MNM.0b013e32833823ac.
9. Shreve PD, Anzai Y, Wahl RL. Pitfalls in oncologic diagnosis with FDG PET imaging: Physiologic and benign variants. Radiographics. 1999;19:61–77. doi:10.1148/radiographics.19.1.g99ja0761.
10. Smith BA, Smith BD. Biomarkers and Molecular Probes for Cell Death Imaging and Targeted Therapeutics. Bioconjug Chem. 2012;23:1989–2006. doi:10.1021/bc3003309.
11. Zhang DJ, Jin QM, Jiang CH, Gao M, Ni YC, Zhang J. Imaging Cell Death: Focus on Early Evaluation of Tumor Response to Therapy. Bioconjug Chem. 2020;31:1025–51. doi:10.1021/acs.bioconjchem.0c00119.
12. Zhang DJ, Gao M, Jin QM, Ni YC, Zhang J. Updated developments on molecular imaging and therapeutic strategies directed against necrosis. Acta Pharmaceutica Sinica B. 2019;9:455–68. doi:10.1016/j.apsb.2019.02.002.
13. 10.1158/1078-0432.Ccr-07-0922
Al-Ejeh F, Darby JM, Brown MP. The La autoantigen is a malignancy-associated cell death target that is induced by DNA-damaging drugs. Clinical cancer research: an official journal of the American Association for Cancer Research. 2007;13:5509s-18 s. doi:10.1158/1078-0432.Ccr-07-0922.
14. Sommer G, Rossa C, Chi AC, Neville BW, Heise T. Implication of RNA-Binding Protein La in Proliferation, Migration and Invasion of Lymph Node-Metastasized Hypopharyngeal SCC Cells. Plos One. 2011;6. doi:10.1371/journal.pone.0025402.
15. Trotta R, Vignudelli T, Candini O, Intine RV, Pecorari L, Guerzoni C, et al. BCR/ABL activates mdm2 mRNA translation via the La antigen. Cancer cell. 2003;3:145–60.
16. Al-Ejeh F, Darby JM, Tsopelas C, Smyth D, Manavis J, Brown MP. APOMAB (R), a La-Specific Monoclonal Antibody, Detects the Apoptotic Tumor Response to Life-Prolonging and DNA-Damaging Chemotherapy. Plos One. 2009;4. doi:10.1371/journal.pone.0004558.
17. Al-Ejeh F, Darby JM, Brown MP. Chemotherapy Synergizes with Radioimmunotherapy Targeting La Autoantigen in Tumors. Plos One. 2009;4. doi:10.1371/journal.pone.0004630.
18. Al-Ejeh F, Darby JM, Pensa K, Diener KR, Hayball JD, Brown MP. In vivo targeting of dead tumor cells in a murine tumor model using a monoclonal antibody specific for the la autoantigen. Clin Cancer Res. 2007;13:5519S-27S. doi:10.1158/1078-0432.Ccr-07-0964.
19. Al-Ejeh F, Staudacher AH, Smyth DR, Darby JM, Denoyer D, Tsopelas C, et al. Postchemotherapy and tumor-selective targeting with the La-specific DAB4 monoclonal antibody relates to apoptotic cell clearance. J Nucl Med. 2014;55:772–9. doi:10.2967/jnumed.113.130559.
20. Staudacher AH, Al-Ejeh F, Fraser CK, Darby JM, Roder DM, Ruszkiewicz A, et al. The La antigen is over-expressed in lung cancer and is a selective dead cancer cell target for radioimmunotherapy using the La-specific antibody APOMAB (R). Ejnmmi Research. 2014;4. doi:10.1186/2191-219x-4-2.
21. Staudacher AH, Bezak E, Borysenko A, Brown MP. Targeted alpha-therapy using 227Th-APOMAB and cross-fire antitumour effects: preliminary in-vivo evaluation. Nucl Med Commun. 2014;35:1284–90.

doi:10.1097/MNM.0000000000000199.

22. Staudacher AH, Liapis V, Brown MP. Therapeutic targeting of tumor hypoxia and necrosis with antibody α-radioconjugates. Antibody Therapeutics. 2018;1:55–63. doi:10.1093/abt/tby010.
23. Jauw YWS, Menke-van der Houven van Oordt CW, Hoekstra OS, Hendrikse NH, Vugts DJ, Zijlstra JM, et al. Immuno-Positron Emission Tomography with Zirconium-89-Labeled Monoclonal Antibodies in Oncology: What Can We Learn from Initial Clinical Trials? Frontiers in Pharmacology 2016;7. doi:10.3389/fphar.2016.00131.
24. Knowles SM, Wu AM. Advances in immuno-positron emission tomography: antibodies for molecular imaging in oncology. Journal of clinical oncology: official journal of the American Society of Clinical Oncology. 2012;30:3884–92. doi:10.1200/JCO.2012.42.4887.
25. Liapis V, Zinonos I, Labrinidis A, Hay S, Ponomarev V, Panagopoulos V, et al. Anticancer efficacy of the hypoxia-activated prodrug evofosfamide (TH-302) in osteolytic breast cancer murine models. Cancer Med. 2016;5:534–45. doi:10.1002/cam4.599.
26. Liapis V, Labrinidis A, Zinonos I, Hay S, Ponomarev V, Panagopoulos V, et al. Hypoxia-activated pro-drug TH-302 exhibits potent tumor suppressive activity and cooperates with chemotherapy against osteosarcoma. Cancer Lett. 2015;357:160–9. doi:10.1016/j.canlet.2014.11.020.
27. Zinonos I, Labrinidis A, Lee M, Liapis V, Hay S, Ponomarev V, et al. Apomab, a fully human agonistic antibody to DR5, exhibits potent antitumor activity against primary and metastatic breast cancer. Mol Cancer Ther. 2009;8:2969–80. doi:10.1158/1535-7163.mct-09-0745.
28. Staudacher AH, Li Y, Liapis V, Hou JJC, Chin D, Dolezal O, et al. APOMAB Antibody-Drug Conjugates Targeting Dead Tumor Cells are Effective In Vivo. Mol Cancer Ther. 2019;18:335–45. doi:10.1158/1535-7163.Mct-18-0842.
29. Hezareh M, Hessell AJ, Jensen RC, van de Winkel JG, Parren PW. Effector function activities of a panel of mutants of a broadly neutralizing antibody against human immunodeficiency virus type 1. Journal of virology. 2001;75:12161–8. doi:10.1128/jvi.75.24.12161-12168.2001.
30. Holland JP, Sheh Y, Lewis JS. Standardized methods for the production of high specific-activity zirconium-89. Nucl Med Biol. 2009;36:729–39. doi:10.1016/j.nucmedbio.2009.05.007.
31. Vosjan M, Perk LR, Visser GWM, Budde M, Jurek P, Kiefer GE, et al. Conjugation and radiolabeling of monoclonal antibodies with zirconium-89 for PET imaging using the bifunctional chelate p-isothiocyanatobenzyl-desferrioxamine. Nat Protoc. 2010;5:739–43. doi:10.1038/nprot.2010.13.
32. Lindmo T, Boven E, Cuttitta F, Fedorko J, Bunn PA. Jr. Determination of the immunoreactive fraction of radiolabeled monoclonal antibodies by linear extrapolation to binding at infinite antigen excess. J Immunol Methods. 1984;72:77–89. doi:10.1016/0022-1759(84)90435-6.
33. Staudacher AH, Li Y, Liapis V, Hou JJC, Chin D, Dolezal O, et al. APOMAB(R) antibody drug conjugates targeting dead tumor cells are effective in vivo. Mol Cancer Ther. 2018. doi:10.1158/1535-7163.Mct-18-0842.
34. Yushkevich PA, Piven J, Hazlett HC, Smith RG, Ho S, Gee JC, et al. User-guided 3D active contour segmentation of anatomical structures: significantly improved efficiency and reliability. Neuroimage.

2006;31:1116–28. doi:10.1016/j.neuroimage.2006.01.015.

35. Sharma SK, Chow A, Monette S, Vivier D, Pourat J, Edwards KJ, et al. Fc-Mediated Anomalous Biodistribution of Therapeutic Antibodies in Immunodeficient Mouse Models. Can Res. 2018;78:1820–32. doi:10.1158/0008-5472.can-17-1958.
36. Moroz A, Lee C-Y, Wang Y-H, Hsiao JC, Sevillano N, Truillet C, et al. A Preclinical Assessment of (89)Zr-atezolizumab Identifies a Requirement for Carrier Added Formulations Not Observed with (89)Zr-C4. Bioconjugate chemistry. 2018;29:3476–82. doi:10.1021/acs.bioconjchem.8b00632.
37. England CG, Jiang D, Ehlerding EB, Rekoske BT, Ellison PA, Hernandez R, et al. (89)Zr-labeled nivolumab for imaging of T-cell infiltration in a humanized murine model of lung cancer. Eur J Nucl Med Mol Imaging. 2018;45:110–20. doi:10.1007/s00259-017-3803-4.
38. Nahmias C, Hanna WT, Wahl LM, Long MJ, Hubner KF, Townsend DW. Time course of early response to chemotherapy in non-small cell lung cancer patients with 18F-FDG PET/CT. J Nucl Med. 2007;48:744–51. doi:10.2967/jnumed.106.038513.
39. Kremerskothen J, Nettermann M, Op De Bekke A, Bachmann M, Brosius J. Identification of human autoantigen La/SS-B as BC1/BC200 RNA-binding protein. DNA Cell Biol. 1998;17:751–9. doi:10.1089/dna.1998.17.751.
40. Barr MP, Gray SG, Hoffmann AC, Hilger RA, Thomale J, O'Flaherty JD, et al. Generation and characterisation of cisplatin-resistant non-small cell lung cancer cell lines displaying a stem-like signature. PLoS One. 2013;8:e54193. doi:10.1371/journal.pone.0054193.
41. 10.1016/j.cyto.2016.06.006
Grimaldi C, Finco D, Fort MM, Gliddon D, Harper K, Helms WS, et al. Cytokine release: A workshop proceedings on the state-of-the-science, current challenges and future directions. Cytokine. 2016;85:101-8. doi:10.1016/j.cyto.2016.06.006.
42. Abou DS, Ku T, Smith-Jones PM. In vivo biodistribution and accumulation of Zr-89 in mice. Nucl Med Biol. 2011;38:675–81. doi:10.1016/j.nucmedbio.2010.12.011.
43. Burvenich IJG, Lee F-T, Guo N, Gan HK, Rigopoulos A, Parslow AC, et al. In Vitro and In Vivo Evaluation of (89)Zr-DS-8273a as a Theranostic for Anti-Death Receptor 5 Therapy. Theranostics. 2016;6:2225–34. doi:10.7150/thno.16260.
44. Bailly C, Gouard S, Guerard F, Chalopin B, Carlier T, Faivre-Chauvet A, et al. What is the Best Radionuclide for Immuno-PET of Multiple Myeloma? A Comparison Study Between (89)Zr- and (64)Cu-Labeled Anti-CD138 in a Preclinical Syngeneic Model. Int J Mol Sci. 2019;20. doi:10.3390/ijms20102564.
45. Zhang Y, Hong H, Cai W. PET tracers based on Zirconium-89. Current radiopharmaceuticals. 2011;4:131–9.
46. Wei WJ, Ni DL, Ehlerding EB, Luo QY, Cai WB. PET Imaging of Receptor Tyrosine Kinases in Cancer. Mol Cancer Ther. 2018;17:1625–36. doi:10.1158/1535-7163.Mct-18-0087.
47. Rudd SE, Roselt P, Cullinane C, Hicks RJ, Donnelly PS. A desferrioxamine B squaramide ester for the incorporation of zirconium-89 into antibodies. Chem Commun. 2016;52:11889–92.

doi:10.1039/c6cc05961a.

48. Raave R, Sandker G, Adumeau P, Jacobsen CB, Mangin F, Meyer M, et al. Direct comparison of the in vitro and in vivo stability of DFO, DFO* and DFOcyclo* for Zr-89-immunoPET. Eur J Nucl Med Mol Imaging. 2019;46:1966–77. doi:10.1007/s00259-019-04343-2.
49. Dijkers EC, Munnink THO, Kosterink JG, Brouwers AH, Jager PL, de Jong JR, et al. Biodistribution of Zr-89-trastuzumab and PET Imaging of HER2-Positive Lesions in Patients With Metastatic Breast Cancer. Clin Pharmacol Ther. 2010;87:586–92. doi:10.1038/clpt.2010.12.
50. Borjesson PK, Jauw YW, de Bree R, Roos JC, Castelijns JA, Leemans CR, et al. Radiation dosimetry of 89Zr-labeled chimeric monoclonal antibody U36 as used for immuno-PET in head and neck cancer patients. J Nucl Med. 2009;50:1828–36. doi:10.2967/jnumed.109.065862.
51. Socinski MA, Jotte RM, Cappuzzo F, Orlandi F, Stroyakovskiy D, Nogami N, et al. Atezolizumab for First-Line Treatment of Metastatic Nonsquamous NSCLC. N Engl J Med. 2018;378:2288–301. doi:10.1056/NEJMoa1716948.
52. Gandhi L, Rodriguez-Abreu D, Gadgeel S, Esteban E, Felip E, De Angelis F, et al. Pembrolizumab plus Chemotherapy in Metastatic Non-Small-Cell Lung Cancer. N Engl J Med. 2018;378:2078–92. doi:10.1056/NEJMoa1801005.
53. Wang Y, Deng W, Li N, Neri S, Sharma A, Jiang W, et al. Combining Immunotherapy and Radiotherapy for Cancer Treatment: Current Challenges and Future Directions. Front Pharmacol. 2018;9:185. doi:10.3389/fphar.2018.00185.

Figures

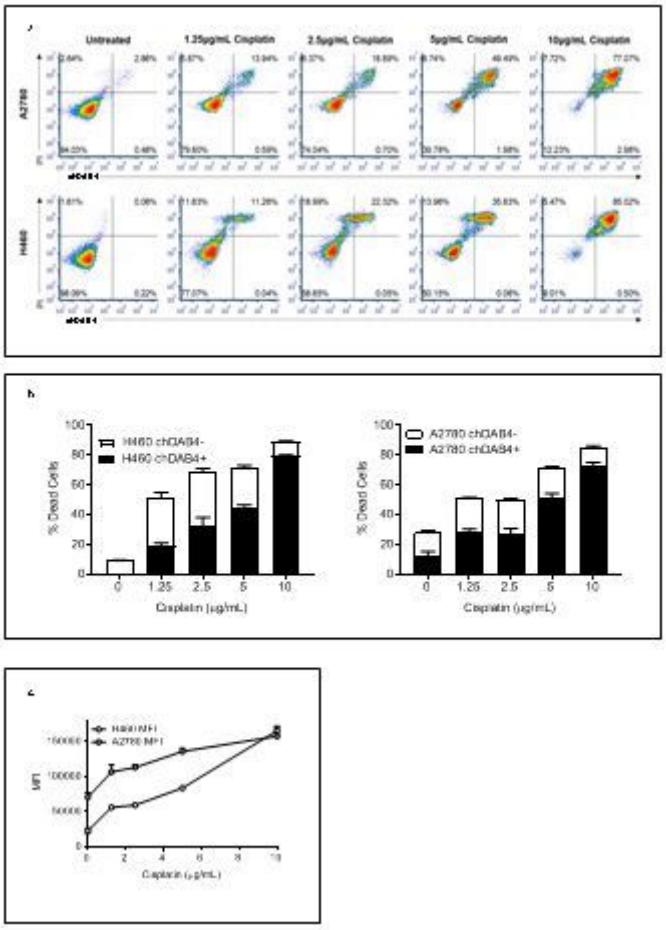

Figure 1

chDAB4 binds to human A2780 ovarian cancer and H460 lung cancer cells after cisplatin treatment in vitro. In both lines, a cisplatin-dose dependent increase in tumor cell death was measured as increased Propidium Iodide positivity (PI+), which corresponded to chDAB4 binding in the flow cytometry density plots (a). Increasing the concentration of cisplatin resulted in increased cell death and chDAB4 binding for both A2780 and H460 cells. (b). After subtracting the mean fluorescence intensity (MFI) of binding of the isotype control (Intragram P), the MFI of chDAB4 bound to PI+ H460 or A2780 cells increased with cisplatin treatment (c). All data points are means ± SD.

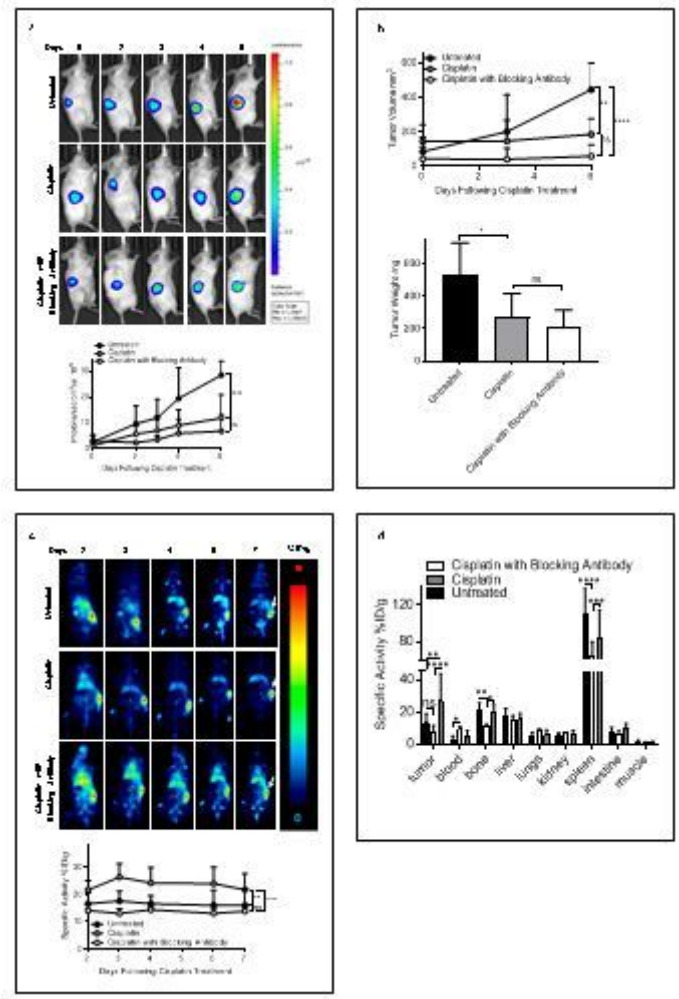

Figure 2

Biodistribution of [89Zr]Zr-chDAB4 in mice bearing subcutaneous xenografts of H460 human lung cancer. Representative longitudinal whole-body bioluminescence images of a single mouse from each group (n = 5) are shown. Color scales indicates relative luminescence (photon flux). The line graph shows relative tumor growth measured as the average tumor bioluminescence signal over time (expressed as mean photon counts per second per cm2) (a). The tumor volume calculated from caliper dimensions on Days 0, 3 and 6 (top panel) and the weight of tumors removed at end of study on Day 7 (bottom panel) (b). Representative longitudinal whole-body PET images of a single mouse from each group are shown. Arrows at Day 7 time point indicate tumors in right flank of each mouse (c). Tumor uptake of [89Zr]Zr-chDAB4 during the experiment was quantified and expressed as the percentage injected dose per gram (%ID/g) using PMOD® software (bottom panel). Organs were removed on Day 7 and the biodistribution of [89Zr]Zr-chDAB4 was measured using a HIDEX counter (right-hand panel) (d). All data points are means ± SD and P values were determined by two-way ANOVA.

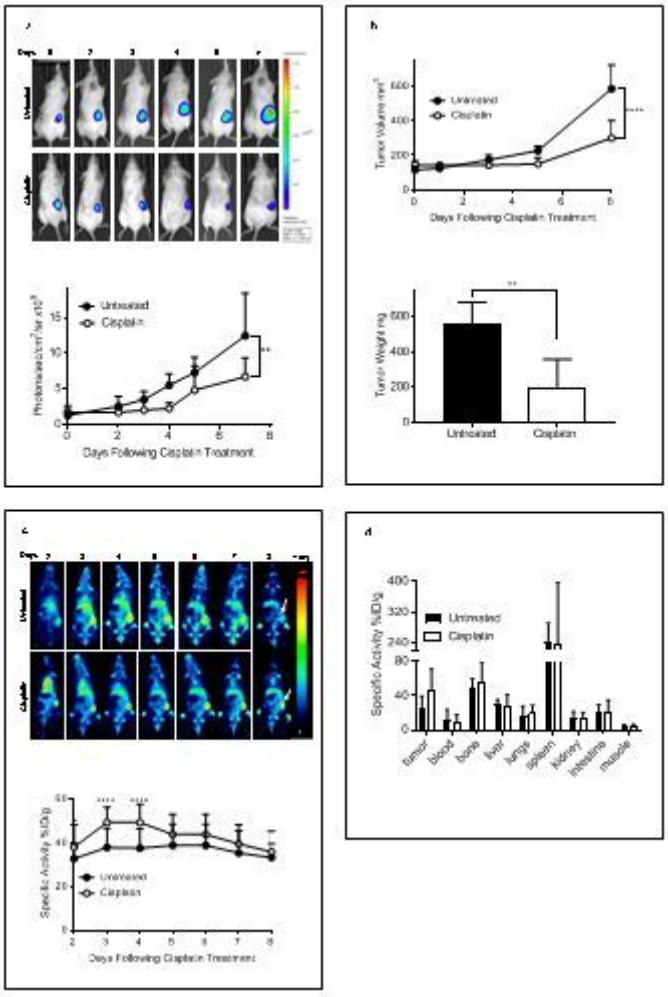

Figure 3

Biodistribution of [89Zr]Zr-chDAB4 in mice bearing subcutaneous xenografts of A2780 human ovarian cancer. Representative longitudinal whole-body bioluminescence images of a single mouse from each group (n = 5) are shown. Color scales indicate relative luminescence (photon flux). The line graph shows average tumor bioluminescence signal over time, expressed as mean photon counts per second per cm2 (a). Tumor volume by caliper measurement and tumor weights at the end of study on Day 8 (b). Representative longitudinal whole-body PET images of tumor-bearing mice after i.v.i administration of the [89Zr]Zr-chDAB4 radioconjugate on Day 1. Relative extent of tissue uptake of activity is shown according to the color scale. Arrows at Day 8 indicate tumors in right flank of each mouse (c). Tumor uptake of the [89Zr]Zr-chDAB4 radioconjugates during the course of the experiment was quantified and expressed as the percentage injected dose per gram (%ID/g) using the PMOD® software. Organs were removed on Day 8 and the biodistribution of [89Zr]Zr-chDAB4 was measured using a Hidex counter (d). P values were measured by two-way ANOVA. All data points are means ± SD.

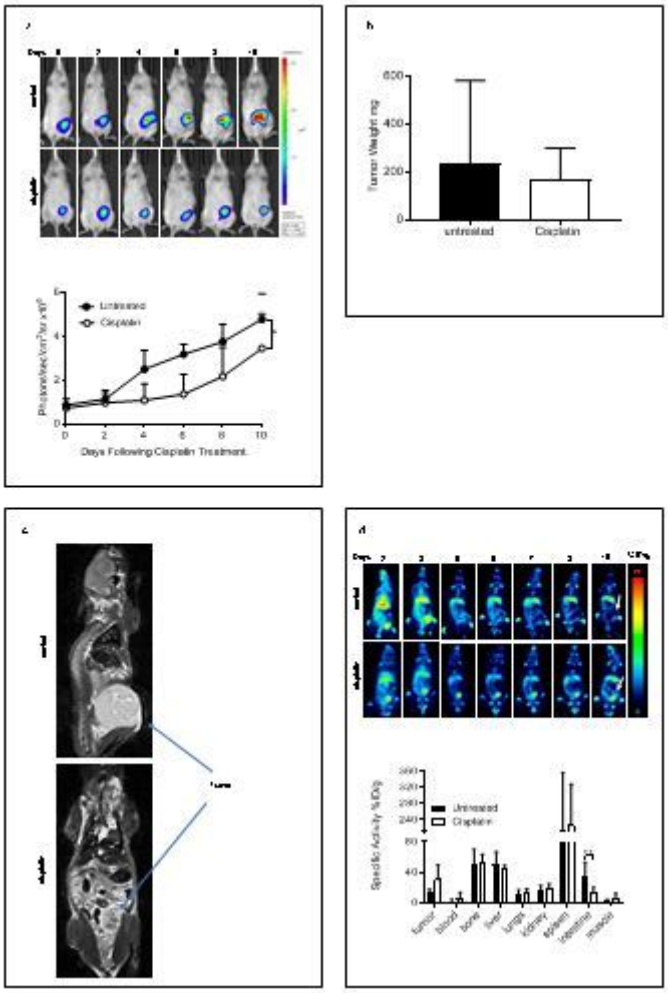

Figure 4

Biodistribution of [89Zr]Zr-chDAB4 in mice bearing ascitic tumors of xenogeneic A2780 human ovarian cancer. Representative longitudinal whole-body bioluminescence images of single mice from each group (n = 3) are shown (top panel) (a). Color scales indicate relative luminescence (or photon flux). Line graph shows average tumor bioluminescence signal over time, expressed as mean photon counts per second per cm2(bottom panel). At the end of the study on Day 10, tumors were removed and weighed (b). MRI scans taken of the same pair of mice show intraperitoneal tumors (arrows) (c). Representative longitudinal whole-body PET images of a single mouse from each group showing the relative extent of tissue uptake of activity are shown. Arrows at Day 10 time point indicate tumors in right flank of each mouse. In the upper control panel, the arrow indicates a PET signal void, which corresponds to the tumor arrowed on the MRI scan. In the lower treatment panel, the arrow marks uptake by the shrunken peritoneal tumor. Organs were removed on Day 10 and the biodistribution of [89Zr]Zr-chDAB4 was measured using a Hidex counter (d). All data points are means ± SD. P values were measured by two-way ANOVA.

Supplementary Files

This is a list of supplementary files associated with this preprint. Click to download.

- supplementaryfigure.pdf